

Plasma Processing for Carbon Nanomaterials. Syntheses of Nanostructures and Their Process Control by Numerical Simulation of Plasma

YOSHIYUKI SUDA, HIROFUMI TAKIKAWA, and HIDETO TANOUE
Toyohashi University of Technology, Japan

SUMMARY

Plasma is a useful tool to synthesize carbon nanomaterials, including diamonds, fullerenes, nanotubes, and graphenes. This review gives an overview of these carbon nanomaterials produced by thermal or nonthermal plasmas and of the authors' work related to plasma-enhanced chemical vapor deposition of carbon nanotubes, along with an analysis and numerical simulation of CH_4/H_2 feedstock gas plasmas. The amount of carbon atoms in the grown carbon nanotubes and that calculated by simulation showed good agreement. © 2013 Wiley Periodicals, Inc. Electron Comm Jpn, 96(6): 1–8, 2013; Published online in Wiley Online Library (wileyonlinelibrary.com). DOI 10.1002/ecj.11504

Key words: plasma-enhanced chemical vapor deposition (PECVD); carbon nanotube (CNT); catalyst; numerical simulation; chemically active species (radical species); flux.

1. Carbon Nanomaterials

1.1 Classification of carbon nanomaterials

The carbon atom contains four unpaired electrons and can have three types of hybrid orbitals: sp^1 , sp^2 , and sp^3

Contract grant sponsors: External Research Funding Project of the Research Center for Future Technology, Toyohashi University of Technology (TUT); by the Research Project of the Venture Business Laboratory (TUT) and the Global COE Program "Frontiers of Intelligent Sensing" of the Ministry of Education, Culture, Sports, Science and Technology (MEXT); by the Core University Programs (JSPS-CAS program in the field of Plasma and Nuclear Fusion) of the Japan Society for the Promotion of Science (JSPS); by a Grand-in-Aid for Scientific Research from JSPS; by the Tokai Foundation for Technology; by the Research Foundation for Materials Science; by the Hori Science and Arts Foundation; and by the Chubu Science and Technology Center.

[1]. Therefore, there are various types of carbon allotropes. Carbyne, with sp^1 bonds, graphite, with sp^2 bonds, and diamond, with sp^3 bonds, are naturally produced [2]. As electron microscopy technique has developed, new carbon allotropes with nanometer-scale structure have been discovered since the 1980s. They are called carbon nanomaterials, referring to their size. In this paper, we select some carbon allotropes and describe their characteristics and the techniques of their synthesis by plasma processing. We have studied plasma-enhanced chemical vapor deposition (PECVD) of carbon nanotubes (CNTs) and the prediction of CNT growth by plasma simulation. Experimental and simulation results are introduced.

1.2 Diamond

Diamond has the highest hardness, Young's modulus, and thermal conductivity of all materials on the earth. The optical transparency of diamond is also high. Taking advantage of these attractive properties, diamond has been regarded as promising for applications in industrial fields, and artificial synthesis methods have been studied for many years. Spitsyn and colleagues in 1981 [3] and Matsumoto and colleagues in 1982 [4] successfully synthesized diamond on a nondiamond substrate in a vapor phase. In the vapor-phase synthesis of diamond, plasma makes a great contribution to the generation of hydrocarbon radicals and atomic hydrogen.

1.3 Fullerene

Fullerene has a spherical shell structure of several tens of carbon atoms, and its shell is composed of five-membered and six-membered rings of carbon atoms. In 1985, Kroto and colleagues synthesized a fullerene with 60 carbon atoms (C_{60}) by laser ablation; this was the discovery of fullerene [5]. Laser ablation is a phenomenon in which atoms and molecules near a solid target are explosively

vaporized by irradiation with intense pulsed laser light and the vaporized particles form a plasma plume [6]. The particles in the plume cool down by colliding with ambient gas molecules and fullerenes and carbon nanotubes are synthesized in the gas ambient.

1.4 Carbon nanotubes

Fullerene was first discovered by a laser ablation experiment and was then found to be synthesizable by an arc discharge. In 1991, Iijima discovered a rolled-up graphite sheet in which six-membered rings of sp^2 -bonded carbon atoms formed a two-dimensional network [7]. This structure was called a carbon nanotube (CNT). The first-discovered CNT was a multiwalled CNT (MWCNT), in which several graphite sheets were nested and formed concentric cylinders. In 1993, a single-walled CNT (SWCNT) was discovered, also by Iijima and Ichihashi [8]. The characteristics of CNTs are as follows: (1) ultrafine carbon fiber with high graphitic crystallinity; (2) ability to emit electrons in a low electric field; (3) superior electrical conductivity and mechanical properties; (4) SWCNT can have either metallic or semiconducting properties depending on the chirality, which is an index of the six-membered ring arrangement in the CNT circumferential direction. Due to these attractive characteristics of CNTs, they are regarded as promising for applications to structural materials, flat-panel displays, interconnection in large-scale integration (LSI), and energy devices.

1.5 Graphene

A single layer of planar graphite sheet is called a graphene. In 2004, Novoselov, Geim, and colleagues peeled off highly-oriented pyrolytic graphite (HOPG) with adhesive tape and formed a few-layer graphene sheet on a substrate. This sheet exhibited a quite high electron mobility, in the vicinity of $10,000 \text{ cm}^2/\text{V}\cdot\text{s}$ [9], and at once attracted attention because it showed potential for application in electronic device fields where CNTs have been regarded as promising. A prototype graphene transparent touch panel has already been created and the application development of graphene is being undertaken at high speed. Hydrocarbon gas plasmas are attracting attention because they can be used to synthesize large-area graphenes at low temperatures [10].

2. Plasma Processing of Carbon Nanomaterials

If we classify the plasmas for carbon nanomaterial processing by the kinetic energy of the particles present, we can identify two types of plasma: thermal plasmas (arc discharge and laser ablation) and low-temperature plasmas

(glow discharge). The difference between them is briefly described below.

2.1 Arc discharge and laser ablation

The difference between the two plasma types comes from the plasma source; they are regarded as identical thermal plasmas in materials processing. In an arc discharge, a large current of several tens of amperes is passed between electrodes with a gap voltage near the ionization voltage of the feedstock gas molecules while thermal electrons are emitted from the cathode. This causes the solid carbon electrode to vaporize, and the vaporized atoms and molecules form fullerenes and CNTs after cooling by collision with ambient gas molecules. CNTs are synthesized if a minute amount of catalyst which forms a solid solution with carbon is included in the carbon electrode. The ambient gases and their pressures differ depending on the processing apparatus. Generally, He, Ar, and N_2 gases are used at pressures of hundreds of hPa.

2.2 Glow discharge and plasma-enhanced chemical vapor deposition (PECVD)

Chemical vapor deposition (CVD) is a chemical process that dissociates feedstock gas molecules on a substrate and forms thin films and fine particles. CVD utilizes thermal and catalytic reactions for dissociation. In PECVD the dissociation reaction is assisted by plasma. Generally, a glow discharge is used as the plasma source of PECVD. All the carbon nanomaterials covered in this paper except fullerenes can be synthesized by PECVD as well as by CVD. In CVD, all types of hydrocarbon gases and alcohol vapors can be used as feedstocks for carbon nanomaterials, and the range of possible growth parameters has been extended. For instance, it is reported that SWCNT has been grown in a very wide range of gas pressures from 10^{-1} (CVD [11]) to 1×10^5 Pa (PECVD [12]). At 10^{-1} Pa, the plasma is no longer sustained, but this low-pressure process moves the possible growth temperature of CNT down to $400 \text{ }^\circ\text{C}$ [11], which is useful for processes in which the temperature range is limited, such as LSI fabrication. In contrast, it was found that a stable glow discharge plasma can be generated and sustained even at an atmospheric pressure [13]. The process utilizing atmospheric-pressure plasma does not require a vacuum pumping system and related instruments, and this makes the processing apparatus simple and inexpensive. Nozaki and colleagues used a $\text{He}/\text{H}_2/\text{CH}_4$ gas mixture that reduced the CH_4 partial pressure and successfully synthesized SWCNT by atmospheric pressure PECVD [12]. It is quite important that the flow rate of the hydrocarbon gas is controlled depending on the molar quantity of carbon nanomaterial growth.

3. Growth Control of Carbon Nanomaterials by Utilizing Plasma Numerical Simulation

3.1 CNT processing apparatus

The PECVD processing apparatus used for CNT synthesis is next briefly outlined. The details of the vacuum chamber and electrode configuration have been described in an earlier paper [14]. The powered electrode was connected to a 13.56-MHz radio frequency (RF) generator through a matching unit. We used infrared heating equipment (Thermo Riko Co. Ltd., GVL298) capable of very quickly raising the temperature (150 °C/s). Gases (CH_4 and H_2) were fed at flow rates that were controlled by mass flow controllers. We used Si substrates covered with a 20-nm-thick SiO_2 layer, and deposited the catalyst (Fe) and its support (Al_2O_3) on the substrate with an electron beam evaporator. We formed triple-layered catalyst films ($\text{Al}_2\text{O}_3/\text{Fe}/\text{Al}_2\text{O}_3 = 1/1/1$ nm) for CNT growth. The catalyst film was applied to the grounded electrode. In PECVD, the catalyst film was processed by 665-Pa H_2 plasma. After this process, we grew CNTs with a 1330-Pa CH_4/H_2 plasma at 650 °C. The experimental conditions are listed in Table 1 [14–16]. We evaluated the CNTs and catalysts by scanning electron microscopy (SEM), transmission electron microscopy (TEM), and X-ray photoelectron spectroscopy (XPS).

3.2 CNT growth model

In CNT growth by PECVD and CVD, a two-stage process—(1) catalyst pretreatment and (2) CNT growth—is used. Figure 1 shows a diagram of CNT growth by PECVD. First, the substrate on which the catalyst layer or catalyst/support multilayer has been formed is pretreated in H_2 plasma. By pretreatment, catalyst/support nanoparticles are formed, and the oxidized catalyst is reduced [16, 17]. After pretreatment, a hydrocarbon gas plasma is generated for CNT growth. In the plasma, the feedstock particles, including neutral particles (nonradical neutrals, e.g., CH_4), positive ions (e.g., CH_4^+), and radicals (e.g., CH_3), are produced and fall onto the catalyst nanoparticles. The number of particles obtained by multiplying their sticking coefficients is counted as the number of particles which are adsorbed onto the surface of the catalyst nanoparticles and dissociate

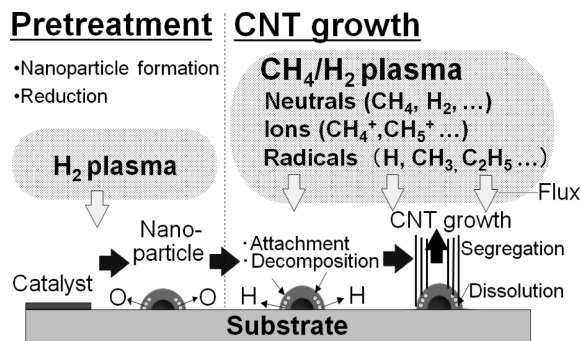


Fig. 1. Diagram of CNT growth by PECVD.

into C and H atoms. The dissociated C atoms are dissolved in the catalyst nanoparticles. When the carbon amount in the catalyst nanoparticles becomes supersaturated, a graphite cap is formed on the surface of the catalyst nanoparticles and CNTs are grown, following the graphite cap. There is a correlation between the CNT and catalyst nanoparticle diameters [18], and this model is widely supported.

If excess C atoms are fed to the surface of the catalyst nanoparticles, the catalyst becomes deactivated and CNTs are no longer grown. In most cases, Fe, Ni, and Co atoms which can dissociate hydrocarbon molecules and dissolve C atoms are used as CNT catalysts. It is reported that Au, Ag, and Cu atoms which cannot dissolve carbon can be used as CNT catalysts when alcohols, which are easy to pyrolyze, are used as a feedstock and the flow rate is controlled with a high degree of accuracy [19]. One of the greatest advantages of PECVD for carbon nanomaterial growth is in feeding a number of chemically active species to catalyst nanoparticles. Control of their quantity is quite important for precise control of the diameter, length, and number density of the CNTs.

3.3 CNT growth results

Figure 2 shows the dependence of CNT growth on the CH_4/H_2 ratio. The growth time was 10 minutes. The CNTs are vertically aligned with a high number density and their length varies with the CH_4/H_2 ratio. Figure 3 shows a TEM micrograph of CNTs obtained at $\text{CH}_4/\text{H}_2 = 21/9$ sccm. The inner and outer diameters of CNTs were measured in the TEM micrographs. The CNTs obtained in this study were almost all multiwalled CNTs (MWCNT). We defined the diameters of the outermost and innermost layers as the CNT outer diameter (d_{outer}) and inner diameter (d_{inner}), respectively. Figure 4 shows the distribution of d_{inner} and d_{outer} . At $\text{CH}_4/\text{H}_2 = 30/0$ sccm, we obtained $d_{\text{inner}} = 2.0$ to 8.0 nm, $d_{\text{outer}} = 4.0$ to 14.0 nm. The thinnest CNT in this study ($d_{\text{inner}} = 1.5$ to 6.0 nm, $d_{\text{outer}} = 2.0$ to 11.0 nm) was obtained

Table 1. PECVD experimental conditions [14–16]

	Pretreatment	Growth process
Pressure	H_2 5 Torr	CH_4/H_2 10 Torr
Flow rate	50 sccm	3–30 / 0–27 sccm
Temperature	550°C	600–750°C

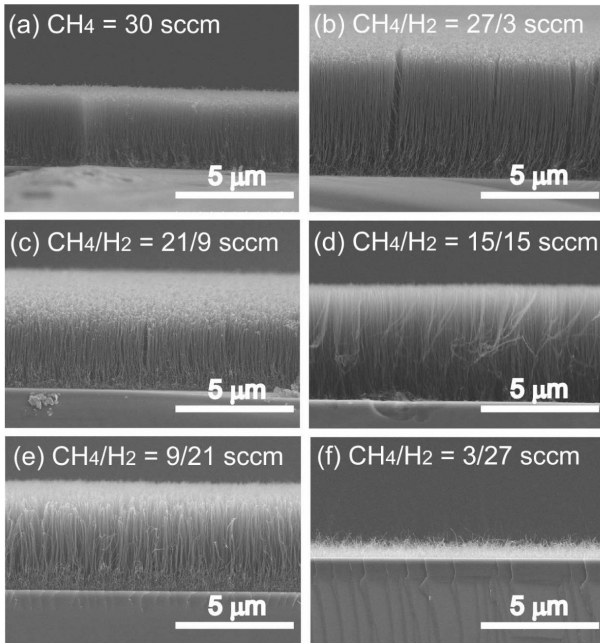


Fig. 2. Dependence of CNT growth on CH_4/H_2 mixture ratio. CH_4/H_2 ratios: (a) 30/0 sccm, (b) 27/3 sccm, (c) 21/9 sccm, (d) 15/15 sccm, (e) 9/21 sccm, and (f) 3/27 sccm (total flow rate was kept constant at 30 sccm) [14].

at $\text{CH}_4/\text{H}_2 = 27/3$ sccm. However, as the H_2 flow rate increased, both d_{inner} and d_{outer} increased.

Let us now discuss the variation of d_{outer} with the CH_4/H_2 ratio. Though we still do not have evidence that explains this phenomenon, XPS analysis results [16] suggest that the Fe catalyst film which was sandwiched between Al_2O_3 support films was oxidized (Fe_2O_3 and/or Fe_3O_4) before pretreatment and gradually reduced as the sandwich film was converted to nanoparticles, after which CNT growth was produced. Under our experimental conditions, there were two oxidation states of Fe (Fe_2O_3 and Fe_3O_4) 4 minutes after pretreatment [16].

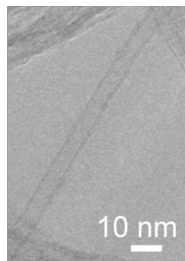


Fig. 3. TEM micrograph of CNTs obtained by CH_4/H_2 (= 21/9 sccm) plasma [14].

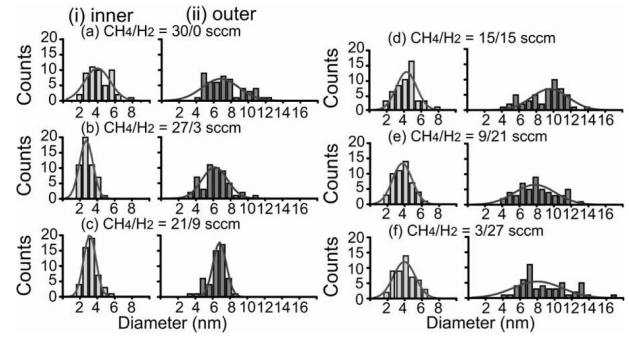


Fig. 4. Frequency distributions of (i) inner diameter and (ii) outer diameter of multiwalled CNTs on the gas mixture ratio: $\text{CH}_4/\text{H}_2 =$ (a) 30/0 sccm, (b) 27/3 sccm, (c) 21/9 sccm, (d) 15/15 sccm, (e) 9/21 sccm, and (f) 3/27 sccm. Fitting curves in these graphs are Gaussian [14].

Also in the CNT growth period, catalyst reduction proceeds further by dissociation of hydrocarbon molecules into C and H atoms on the catalyst surface. Catalyst reduction causes a decrease of the number of Fe atoms composing the catalyst nanoparticles, and the catalyst nanoparticles become small. However, if catalyst reduction proceeds too far, the catalyst nanoparticles tend to coagulate and instead become large. This makes the CNT diameter increase. Based on this consideration, at $\text{CH}_4/\text{H}_2 = 27/3$ sccm, neither excess hydrocarbon molecules that cause catalyst deactivation nor excess H radicals that cause catalyst nanoparticle coagulation were supplied, and the CNT diameter became small. By contrast, at $\text{CH}_4/\text{H}_2 = 30/0$ sccm, excess hydrocarbon radicals were supplied, and the CNT diameter became large. When many H_2 molecules were supplied, such as at $\text{CH}_4/\text{H}_2 = 9/21$ sccm, the coagulation of catalyst nanoparticles occurred. This resulted in thick CNT growth. In the results for $\text{CH}_4/\text{H}_2 = 15/15$ sccm, 9/21 sccm, and 3/27 sccm in Figs. 4 (d), (e), (f), the CNT diameter distribution became broader with an increasing H_2 flow rate ratio. This suggests that the diameters of the catalyst nanoparticles were dispersed.

We examined the dependence of the CNT growth period on the CH_4/H_2 gas flow rate ratio as shown in Fig. 5. At $\text{CH}_4/\text{H}_2 = 30/0$ sccm, CNTs grew at a higher rate ($R_{\text{CNT}} = \sim 0.8 \mu\text{m}/\text{min}$) than under other conditions until 30 minutes. However, CNT growth became saturated at times longer than 30 minutes. At $\text{CH}_4/\text{H}_2 = 27/3$ sccm, CNTs continued to grow for 90 minutes (growth rate = $0.3 \mu\text{m}/\text{min}$). At $\text{CH}_4/\text{H}_2 = 9/21$ sccm, CNT growth was saturated before 10 minutes. These results show that the CNT growth period was greatly changed by adding H_2 gas to CH_4 gas at a mixture ratio of only 10%. Also, the incubation periods for CNT growth are expected to differ according to the results in Fig. 5, because the initial CNT lengths are

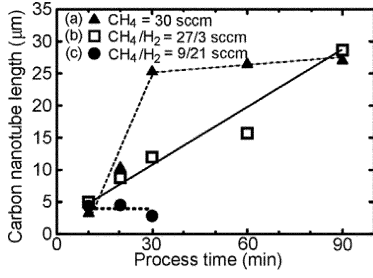


Fig. 5. Dependence of CNT length (L_{CNT}) on process time. CH_4/H_2 ratios were 30/0 sccm (filled triangles), 27/3 sccm (open squares), and 9/21 sccm (filled circles) [14].

different. This suggests the importance of appropriate feedstock supply to appropriately reduced catalyst nanoparticles.

3.4 Plasma fluid modeling

We analyzed CH_4/H_2 plasmas using a one-dimensional fluid code for a parallel-electrode system [14, 15, 20], which had the same dimensions as the CNT processing apparatus (electrode radius 3.2 cm, gap distance 1.5 cm). The simulation consisted of calculations of the continuity equations, the Poisson equation, and the electron energy conservation equation. In the present paper, we added the chemical reactions relevant to H_2 to the previous CH_4 plasma reactions in order to examine the effect of H_2 gas addition to CH_4 gas. The transport coefficients and the reaction rates of electrons had to be calculated because the electron energy distribution was changed by the addition of H_2 to CH_4 . To calculate the transport coefficient and reac-

tion rate of electrons, we used a Boltzmann equation solver (BOLSIG+) [14] and solved the Boltzmann equation using a H_2 cross-section set. We added this calculation result to this analysis. We considered 10 charged particles (e^- , H_2^+ , H_3^+ , CH_3^+ , CH_4^+ , CH_5^+ , C_2H_2^+ , C_2H_4^+ , C_2H_5^+ , C_2H_6^+), five radicals (H , CH , CH_2 , CH_3 , C_2H_5), six nonradical neutrals (H_2 , CH_4 , C_2H_2 , C_2H_4 , C_2H_6 , C_3H_8). One hundred twenty-seven reactions in this CH_4/H_2 plasma simulation (electron-neutral, neutral-neutral, ion-neutral, and electron-neutral reactions) were included in this calculation. We also considered sticking probabilities ($s_{\text{CH}} = 0.025$, $s_{\text{CH}_2} = 0.025$, $s_{\text{CH}_3} = 0.01$, $s_{\text{C}_2\text{H}_5} = 0.01$, $s_{\text{H}} = 0.001$, $s_{\text{ion}} = 1$, $s_{\text{neutral}} = 0$) [15]. The fluxes of CNT feedstock particles, which were used for evaluation of the C amount on catalyst nanoparticles and are discussed in the next section, were calculated by considering only the particles incident on the catalyst nanoparticles on the substrate in the plasma. If we assume that the plasma in this study is in the thermal equilibrium state, the flux of nonradical neutrals and radicals due to thermal diffusion is expressed as follows:

$$\Gamma = \frac{1}{4} n \langle v \rangle \quad (1)$$

$$\langle v \rangle = \sqrt{\frac{8k_{\text{B}}T}{\pi m}} \quad (2)$$

where n is the species density, $\langle v \rangle$ is the mean thermal velocity, k_{B} is the Boltzmann constant, T is the temperature of nonradical neutrals (gas temperature), and m is the mass of the species [20].

Figure 6 shows the number densities of (a) nonradical neutrals, (b) radical neutrals, and (c) positive ions in the vicinity of the substrate at different CH_4/H_2 gas pressures [20]. As shown by Fig. 6(a), the density of all nonradical neutrals gradually increases with increasing gas pressure. The major gas molecules in the plasma are CH_4 and H_2 ,

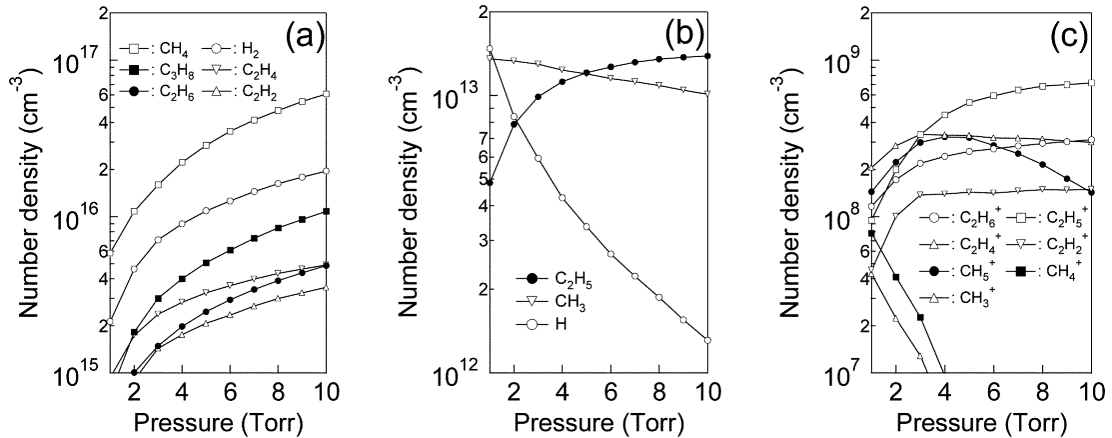


Fig. 6. Pressure dependence of the time-averaged number densities of (a) nonradical neutrals; (b) radical neutrals; and (c) positive ions in the vicinity of the substrate in the CH_4/H_2 plasmas at 1 to 10 torr [20].

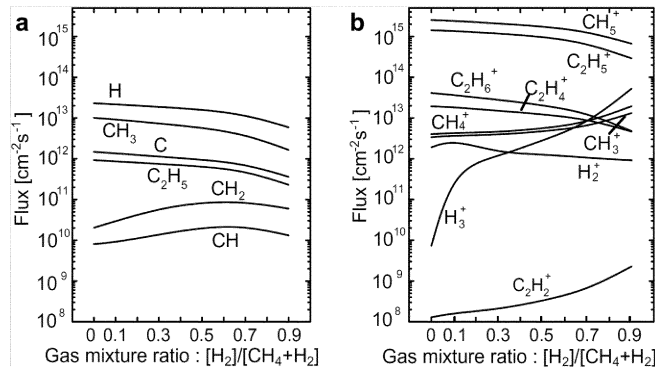


Fig. 7. Dependence of fluxes onto substrate on CH_4/H_2 ratio: fluxes of (a) radical species and (b) ionic species. Total pressure was kept at 10 torr [14].

with a number density of $\sim 10^{16} \text{ cm}^{-3}$, followed by the nonradical neutrals, C_3H_8 , C_2H_4 , and C_2H_6 . The number densities of the radical neutrals, C_2H_5 , and CH_3 , and of positive ions are respectively two and five orders of magnitude smaller than those of the nonradical neutrals [Fig. 6(a) and (c)]. The dependence of the fluxes of radical and ionic species onto the substrate on the CH_4/H_2 ratio is shown in Fig. 7 [14]. For radicals, the fluxes of H and CH_3 are the largest, and for ions, CH_5^+ and C_2H_5^+ are the largest.

As shown in Figs. 2, 4, and 5, CNTs continued to grow for 90 minutes at $\text{CH}_4/\text{H}_2 = 27/3$ sccm. Comparing the result of $[\text{H}_2]/[\text{CH}_4 + \text{H}_2] = 0.1$ with that of $[\text{H}_2]/[\text{CH}_4 + \text{H}_2] = 0$ (pure CH_4) in Fig. 7, H_2^+ and H_3^+ increased appreciably. These species are generated by the direct ionization of H_2 due to electron collision and by charge-exchange collision between H_2 and H_2^+ . H_2 and H_2^+ as well as H radicals, whose flux was one order higher than those of H_2 and H_2^+ , are considered to contribute to catalyst reduction. When $[\text{H}_2]/[\text{CH}_4 + \text{H}_2]$ increased from 0 to 1, the flux of H_3^+ increased by a factor of 10^4 . This

caused excess reduction of catalyst nanoparticles due to the production of H_2 -dominant plasma and suppressed CNT growth.

3.5 Predicting the carbon amount

We estimated the number of C atoms (N_C) per unit substrate area and compared the values predicted by the experimental results with those calculated in the simulation. The details of how to estimate N_C are described in our earlier paper [15]. For experimental prediction of N_C , we assumed that the CNTs consist of a graphite sheet with constant carbon density ($= 3.81 \times 10^{15} \text{ cm}^{-2}$, theoretically). We used the measured values (CNT diameter, CNT length, CNT number density, average number of graphite layers) and estimated N_C in the CNTs. In the simulation, we integrated the fluxes of radicals, ions, and nonradical neutrals incident on the substrate surface. We considered the sticking probabilities of these species containing carbon as weights in the integration. We estimated N_C of the carbon atoms supplied to the substrate surface.

Figure 8 shows the values of N_C obtained experimentally and by simulation. The values from the experiment and the simulation were of the same order of magnitude, and were closest at $\text{CH}_4/\text{H}_2 = 27/3$ sccm. The experimental and simulation results also show good agreement with respect to the decreasing tendency of N_C with the increase of the H_2 - CH_4 mixture ratio.

4. Conclusions

An approach to evaluation of the amount of carbon deposited in PECVD was introduced. This approach is not limited to CNT growth but is also applicable to other carbon nanomaterials, including graphenes. However, fundamental data on the sticking coefficients of radicals are limited

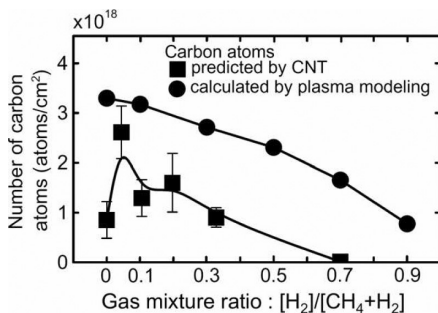


Fig. 8. Comparison of carbon atoms: estimated by experimental method (filled squares) and simulation analysis (filled circles) [14].

and the types of substrates on which the sticking coefficients have been evaluated are limited. By accumulating such experimental and simulation data, prediction of the major species which contribute to carbon nanomaterial synthesis in plasma processing would be made possible.

Acknowledgments

We thank Professor A. Oda of Chiba Institute of Technology for valuable discussions. The experimental and simulation results described in this paper were obtained by Dr. A. Okita of Hitachi High-Technologies Corp. and post-graduate members of Professor Y. Sakai's laboratory at Hokkaido University. This work was supported in part by the External Research Funding Project of the Research Center for Future Technology, Toyohashi University of Technology (TUT); by the Research Project of the Venture Business Laboratory (TUT) and the Global COE Program "Frontiers of Intelligent Sensing" of the Ministry of Education, Culture, Sports, Science and Technology (MEXT); by the Core University Programs (JSPS-CAS program in the field of Plasma and Nuclear Fusion) of the Japan Society for the Promotion of Science (JSPS); by a Grand-in-Aid for Scientific Research from JSPS; by the Tokai Foundation for Technology; by the Research Foundation for Materials Science; by the Hori Science and Arts Foundation; and by the Chubu Science and Technology Center.

REFERENCES

1. Russo S, Silver ME. Introductory chemistry. Benjamin-Cummings; 2001.
2. Kobashi K. Diamond films: Chemical vapor deposition for oriented and heteroepitaxial growth. Elsevier Science; 2005.
3. Spitsyn BV, Bouliv LL, Derajaguin BV. Vapor growth of diamond on diamond and other surfaces. *J Crystal Growth* 1981;52(Part 1):219–226.
4. Matumoto S, Sato Y, Kamo M, Setaka N. Vapor deposition of diamond particles from methane. *Jpn J Appl Phys* 1982;21:L183–L185.
5. Kroto HW, Heath JR, O'Brien SC, Curl RF, Smalley RE. C₆₀: Buckminsterfullerene. *Nature* 1985;318:162–163.
6. Chrisey DB, Hubler GK (editors). Pulsed laser deposition of thin films. Wiley; 1994.
7. Iijima S. Helical microtubules of graphitic carbon. *Nature* 1991;354:56–58.
8. Iijima S, Ichihashi T. Single-shell carbon nanotubes of 1-nm diameter. *Nature* 1993;354:603–605.
9. Novoselov KS, Geim AK, Morozov SV, Jiang D, Zhang Y, Dubonos SV, Grigorieva IV, Firsov AA. Electric field effect in atomically thin carbon films. *Science* 2004;306:666–669.
10. Kim J, Ishihara M, Koga Y, Tsugawa K, Hasegawa M, Iijima S. Low-temperature synthesis of large-area graphene-based transparent conductive films using surface wave plasma chemical vapor deposition. *Appl Phys Lett* 2011;98:091502.
11. Maruyama T, Sato K, Mizutani Y, Tanioku K, Shiraiwa T, Naritsuka S. Low-temperature synthesis of single-walled carbon nanotubes by alcohol gas source growth in high vacuum. *J Nanosci Nanotechnol* 2010;10:4095–4101.
12. Nozaki T, Ohnishi K, Okazaki K, Kortshagen U. Fabrication of vertically aligned single-walled carbon nanotubes in atmospheric pressure non-thermal plasma CVD. *Carbon* 2007;45:364–374.
13. Becker KH, Kogelschatz U, Schoenbach KH, Barker RJ (editors). Non-equilibrium air plasmas at atmospheric pressure (Series in Plasma Physics). Taylor & Francis; 2004.
14. Okita A, Suda Y, Oda A, Nakamura J, Ozeki A, Bhattacharyya K, Sugawara H, Sakai Y. Effects of hydrogen on carbon nanotube formation in CH₄/H₂ plasmas. *Carbon* 2007;45:1518–1526.
15. Okita A, Suda Y, Ozeki A, Sugawara H, Sakai Y, Oda A, Nakamura J. Predicting the amount of carbon in carbon nanotubes grown by CH₄ RF plasmas. *J Appl Phys* 2006;99:014302-1-7.
16. Okita A, Ozeki A, Suda Y, Nakamura J, Oda A, Bhattacharyya K, Sugawara H, Sakai Y. Analysis of oxidation state of multi-layered catalyst thin films for carbon nanotube growth using plasma-enhanced chemical vapor deposition. *Jpn J Appl Phys* 2006;45:8323–8329.
17. de los Arcos T, Garnier MG, Seo JW, Oelhafen P, Thommen V, Mathys D. The influence of catalyst chemical state and morphology on carbon nanotube growth. *J Phys Chem B* 2004;108:7728–7734.
18. Jeong GH, Yamazaki A, Suzuki S, Yoshimura H, Kobayashi Y, Homma Y. Cobalt-filled apoferritin for suspended single-walled carbon nanotube growth with narrow diameter distribution. *JACS* 2005;127:8238–8239.
19. Takagi D, Homma Y, Hibino H, Suzuki S, Kobayashi Y. Single-walled carbon nanotube growth from highly activated metal nanoparticles. *Nano Lett* 2006;6:2642–2645.
20. Oda A, Suda Y, Okita A. Numerical analysis of pressure dependence on carbon nanotube growth in CH₄/H₂ plasmas. *Thin Solid Films* 2008;516:6570–6574.

AUTHORS (from left to right)



Yoshiyuki Suda received his M.E. and Ph.D. degrees in electronic and information engineering from Hokkaido University in 1997 and 2006. He is currently an associate professor in the Department of Electrical and Electronic Information Engineering, Toyohashi University of Technology. He is a member of IEE Japan, the Japan Society of Applied Physics, and the Fullerenes, Nanotubes, and Graphene Research Society.

Hirofumi Takikawa received his M.S. and Ph.D. degrees in engineering from Toyohashi University of Technology in 1986 and 1992. He is now a professor in the Department of Electrical and Electronic Information Engineering of Toyohashi University of Technology. He is a member of IEE Japan and the Japan Society of Applied Physics.

Hideto Tanoue received his M.E. and Ph.D. degrees in electronic and information engineering from Toyohashi University of Technology in 2008 and 2010. He is currently an assistant professor in the Department of Electrical and Electronic Information Engineering, Toyohashi University of Technology. He is a member of IEE Japan, the Japan Society of Applied Physics, and the Surface Finishing Society of Japan.